Reduced streamflow in water-stressed climates consistent with CO_2 effects on vegetation

Anna M. Ukkola[1,2*], I. Colin Prentice[1,3], Trevor F. Keenan[1], Albert I.J.M. van Dijk[4], Neil R. Viney[5], Ranga B. Myneni[6] & Jian Bi[6]

[1]Department of Biological Sciences, Macquarie University, North Ryde, New South Wales 2109, Australia
[2]CSIRO Water for a Healthy Country Flagship, Black Mountain, Australian Capital Territory 2601, Australia
[3]AXA Chair of Biosphere and Climate Impacts, Grand Challenges in Ecosystems and the Environment and Grantham Institute – Climate Change and the Environment, Department of Life Sciences, Imperial College London, Silwood Park Campus, Buckhurst Road, Ascot SL5 7PY, UK
[4]Fenner School of Environment & Society, Australian National University, Canberra, Australian Capital Territory 0200, Australia
[5]CSIRO Land and Water Flagship, Canberra, Australian Capital Territory 2601, Australia
[6]Department of Earth and Environment, Boston University, Boston, MA 02215, USA

*email: amukkola@gmail.com

Global environmental change has implications for the spatial and temporal distribution of water resources, but quantifying its effects remains a challenge. The impact of vegetation responses to increasing atmospheric CO_2 concentrations on the hydrological cycle is particularly poorly constrained[1–3]. Here we combine remotely sensed normalized difference vegetation index (NDVI) data and long-term water-balance evapotranspiration (ET) measurements from 190 unimpaired river basins across Australia during 1982-2010 to show (a) that the precipitation threshold for water limitation of vegetation cover has significantly declined during the past three decades, while (b) sub-humid and semi-arid basins are not only 'greening' but also consuming more water, leading to significant (24–28%) reductions in streamflow. In contrast, wet and arid basins show non-significant changes in NDVI and reductions in ET. These observations are consistent with expected effects of elevated CO_2 on vegetation. They suggest that projected future decreases in precipitation[4] will likely be compounded by increased vegetation water use, further reducing streamflow in water-stressed regions.

Experiments have shown that elevated atmospheric CO_2 affects vegetation productivity and water use[5]. CO_2 is the substrate for photosynthesis and concentrations above current ambient levels stimulate carbon assimilation by plants. This CO_2 fertilisation effect should in principle lead to increased biomass and green vegetation cover ('greening'). Simultaneously, increasing CO_2 lowers stomatal conductance, reducing water loss through leaves. Reduced stomatal conductance and/or stimulated photosynthesis lead to enhanced water use efficiency, the amount of water required to produce a unit of biomass. The effect of CO_2 on vegetation is commonly expected to manifest most strongly in water-limited environments[6,7], where moisture is the main limitation on plant growth. However, not all studies show a strong link between aridity and the strength of the CO_2 effect[8] and the magnitude of associated greening and water savings are generally not well constrained across species and ecosystems[9–11].

CO_2-induced structural and physiological changes in vegetation potentially have consequences for water resources. CO_2 fertilisation and associated greening tends to increase vegetation water consumption by increasing the amount of transpiring leaf area, whereas reduced stomatal conductance tends to decrease transpiration per unit leaf area –two effects with opposing consequences for streamflow[2]. Furthermore, increased vegetation cover can change the partitioning of rainfall into rainfall interception, infiltration and runoff, while shading by increased foliage cover may lead to reductions in soil evaporation by decreasing the amount of radiation reaching the ground surface[12]. It remains unresolved whether these various processes in combination have led to a detectable imprint in ET or streamflow. At the global scale, both decreases and increases in ET due to CO_2 have been reported[1,2] and the results appear to be data- and model-dependent[3]. The direction and magnitude of the CO_2 effect on ET and streamflow thus remains poorly understood at catchment and regional scales. This situation is compounded by difficulties in estimating ET at large scales[13,14].

We investigated the correlates and potential causes of long-term changes in vegetation across Australia using remotely sensed NDVI. NDVI has been found to relate to primary productivity[15], foliage cover[16] and biomass[17] and has been widely employed to quantify vegetation trends[6,18,19] and processes[20]. We also examined long-term changes in ET and streamflow in unregulated, unimpaired Australian river

basins in climates of varying aridity. ET was assessed by the water balance method, which relies directly on observations of precipitation and streamflow.

We first investigated the spatial distribution of long-term changes in NDVI across Australia. Large areas of Australia have undergone greening during 1982-2010 (Figure 1a); precipitation explained about 50% of these trends (calculated as the coefficient of determination from a linear regression of NDVI and precipitation trends). Strong greening was observed particularly in water-limited areas (marked by positive NDVI-precipitation correlation; Figure 1b), where 65% of significant ($P \leq 0.05$) NDVI trends were positive (excluding areas of significant precipitation increase).

We then quantified changes in the vegetation-precipitation relationship in areas of natural and semi-natural vegetation across Australia. By examining temporal changes in the upper 95th percentile bound for the spatial relationship between annual precipitation and NDVI (Figure 2, see Methods) we identified long-term changes in i) the maximum NDVI attainable for a given amount of precipitation, and ii) the extent of vegetation water limitation. We found that the maximum NDVI attainable for a given precipitation level has increased over time in water-limited areas (Figure 3a) ($P = 0.059$). This implies that a given amount of precipitation has sustained greater levels of plant production over time, which is consistent with CO_2 fertilisation. In addition, the breakpoint marking the precipitation limit where vegetation ceases to be water-limited decreased over time ($P = 0.039$) (Figure 3b). This trend indicates a relaxation of vegetation water limitation, consistent with the increased water use efficiency that is expected to accompany rising CO_2.

To analyse long-term changes in vegetation and hydrology at the river basin scale, we calculated CO_2 sensitivity coefficients for NDVI and ET across basins grouped into four aridity categories (wet, sub-humid, semi-arid and arid), as theory would predict that a CO_2 effect should differ systematically between the categories. The sensitivity coefficients express the fractional change in ET and NDVI per unit fractional change in CO_2 concentration (after correcting ET and NDVI for precipitation and potential evapotranspiration (PET) variations, as detailed in Methods). A positive sensitivity coefficient of ET to CO_2 of comparable magnitude to that of NDVI would indicate that a CO_2 stimulation of vegetation cover dominates over a reduction in stomatal conductance with rising CO_2, due to an increased surface area of leaves for transpiration and rainfall interception. A negative sensitivity coefficient of ET to CO_2

(which can be of magnitude up to −1 at high CO_2 concentrations) indicates that the reduction in stomatal conductance with rising CO_2 dominates over the CO_2 stimulation of vegetation cover. We predict theoretical sensitivities around −0.6 in wet climates and −0.4 in arid climates due to the effect of a reduction in stomatal conductance with rising CO_2 on ET (see Methods).

In sub-humid and semi-arid basins, the data show a significant positive sensitivity coefficient of ET and NDVI to CO_2 (0.44 ± 0.14 and 0.18 ± 0.08 for ET, 0.10 ± 0.04 and 0.18 ± 0.11 for NDVI, respectively; Figure 4a). In sub-humid basins, the sensitivity coefficient of ET to CO_2 is similar to the sensitivity coefficient of ET to precipitation (0.64 ± 0.05, calculated from uncorrected data; Supplementary Figure 2a and Supplementary Table 2). In semi-arid basins, the sensitivity coefficient of ET to CO_2 is about a fifth of its sensitivity coefficient to precipitation (0.86 ± 0.02). The CO_2 concentration increased by 48 ppm during the period 1982-2010. Based on the sensitivity coefficients the CO_2-induced ET increases during this time period amount to 43 mm in sub-humid and 14 mm in semi-arid basins, on average. These translate to a 6% and 2% increase, respectively, in mean annual ET (Figure 4b). The relative changes in mean annual ET due to CO_2 are similar to those due to precipitation (-6% and 1%, respectively; Supplementary Figure 2b and Supplementary Table 5) and significantly larger than those due to PET (-1% and 0%, respectively; Supplementary Figure 2b and Supplementary Table 6). Together with significant positive NDVI sensitivity coefficients to CO_2 (Figure 4a), this finding suggests an effect of rising CO_2 on both NDVI and ET, and that the fertilisation effect dominates over stomatal closure.

In wet basins, the sensitivity coefficient of ET to CO_2 was found to be negative (−0.42), consistent with theoretical predictions (see Methods), but this value was not statistically distinguishable from zero (Figure 4a). No greening was detected. In wet environments, vegetation cover is nearly complete and expected to be limited by light and nutrients rather than water. Thus limited greening should occur, and the principal effect of CO_2 on ET would be a decline due to reduced stomatal conductance.

We also found negative but non-significant CO_2 coefficients on ET (–0.33 ± 0.55) and NDVI (–0.11 ± 0.34) in arid basins (Figure 4a). This finding runs counter to the common expectation that CO_2 effects should be most pronounced in the most strongly water-limited environments. However, it is consistent with field experimental evidence showing no long-term change in biomass or water use efficiency under

elevated CO_2 in a desert environment[8]. This lack of a detectable response has been attributed to a high frequency of years with very low precipitation, inhibiting any sustained increase in vegetation biomass[8]. Warm arid areas also tend to harbour a larger proportion of C_4 grasses, which we estimate to cover 43% of the area in arid basins on average (further discussed in Supplementary Section 1). C_4 plants show reduced stomatal conductance under elevated CO_2, consistent with the observed reduction in ET, but the stimulation of photosynthesis in C_4 plants is limited compared to C_3 plants that dominate in cooler and wetter regions[5,21] and only occurs under drought conditions[5]. The high proportion of C_4 vegetation may thus further contribute to the lack of a CO_2 fertilisation effect in arid basins.

We investigated the implications of the long-term ET changes for streamflow. Where ET exceeds streamflow, changes in ET are magnified in streamflow. This was apparent in sub-humid and semi-arid basins, where a small (2-6%) increase in ET led to substantial percentage reductions in streamflow. Calculated streamflow (factoring out precipitation effects) declined during 1982-2010 by 24% in sub-humid basins and by 28% in semi-arid basins (Figure 4b), which, considering the CO_2 sensitivities for these regions, is consistent with a response to CO_2. Given the actual observed declining trend in precipitation in the sub-humid basins (-3 mm/yr^2, $P < 0.001$; Supplementary Figure 4), increasing CO_2 is likely to have aggravated the pressure on water resources in these basins. In arid basins, a 4% decrease in ET would have led to a 132% increase in streamflow and in wet basins a 5% ET decrease would have led to a 5% increase in streamflow. However, neither effect is statistically significant, so we cannot detect a CO_2 effect on streamflow in either the wettest or the driest regions on the basis of these measurements.

Our results provide evidence that rising atmospheric CO_2 has led to observable changes in terrestrial ecosystems and hydrology across a large part of Australia, with implications for carbon and water cycling at regional to global scales. Terrestrial ecosystems worldwide currently withdraw about a quarter of all anthropogenically emitted CO_2 when averaged over a decade[22]. A recent study[23] showed that semi-arid areas, particularly in Australia, play a major regional and even global role in modulating interannual variations in the rate of terrestrial carbon uptake. Increased carbon sequestration rates due to CO_2-induced greening in these semi-arid regions may lead to enhanced uptake of CO_2 from the atmosphere in the future. Furthermore, the response to rising CO_2 has the potential to either magnify or counteract future changes in precipitation. Precipitation is projected to decline in

semi-arid and arid Australia during the 21st century[4] and increasing CO_2 is thus likely to put further pressure on water resources in already water-stressed regions. Our results may have similar implications for other water-limited subtropical regions in the Mediterranean, southern Africa and the Americas where precipitation is also projected to decline with increasing global temperature[4]. We conclude that increasing atmospheric CO_2 has likely left a detectable imprint on Australian ecosystems and hydrology, and such responses should be taken into account in future projections of water resources.

Correspondence and requests for materials should be addressed to A.U.

Acknowledgements

The authors are very grateful to Prof. Michael Hutchinson (Australian National University) and colleagues for providing the climate data used in this study. We would also like to thank Dr. Randall Donohue (CSIRO Land and Water) for useful discussions. A.U. has been supported by an international Macquarie University Research Excellence scholarship and a CSIRO Water for a Healthy Country Flagship top-up scholarship. T.F.K. acknowledges support from a Macquarie University Research Fellowship. This paper is a contribution to the AXA Chair Programme in Biosphere and Climate Impacts, and the Imperial College initiative on Grand Challenges in Ecosystems and the Environment.

Author contributions

I.C.P., A.U. and T.K. designed the research and methodology. A.U. conducted all statistical and graphical analyses. R.M. and N.V. provided the key datasets. A.U. and I.C.P. wrote the first draft; all authors commented on the final manuscript and assisted with data interpretation.

References:

1. Gedney, N. *et al.* Detection of a direct carbon dioxide effect in continental river runoff records. *Nature* **439,** 835–838 (2006).

2. Piao, S. *et al.* Changes in climate and land use have a larger direct impact than rising CO_2 on global river runoff trends. *Proc. Natl. Acad. Sci.* **104,** 15242–15247 (2007).

3. Alkama, R., Decharme, B., Douville, H. & Ribes, A. Trends in global and basin-scale runoff over the late twentieth century: methodological issues and sources of uncertainty. *J. Clim.* **24,** 3000–3014 (2011).

4. Collins, M. *et al.* in *Climate Change 2013: The Physical Science Basis. Contribution of Working Group I to the Fifth Assessment Report of the Intergovernmental Panel on Climate Change* (eds. Stocker, T. F. et al.) 1029–1136 (Cambridge University Press, 2013).

5. Leakey, A. D. B. *et al.* Elevated CO_2 effects on plant carbon, nitrogen, and water relations: six important lessons from FACE. *J. Exp. Bot.* **60,** 2859–2876 (2009).

6. Donohue, R. J., Roderick, M. L., McVicar, T. R. & Farquhar, G. D. Impact of CO_2 fertilization on maximum foliage cover across the globe's warm, arid environments. *Geophys. Res. Lett.* **40,** 1–5 (2013).

7. Hovenden, M. J., Newton, P. C. D. & Wills, K. E. Seasonal not annual rainfall determines grassland biomass response to carbon dioxide. *Nature* **511,** 583–586 (2014).

8. Newingham, B. A. *et al.* No cumulative effect of 10 years of elevated [CO_2] on perennial plant biomass components in the Mojave Desert. *Glob. Chang. Biol.* **19,** 2168–81 (2013).

9. Bradley, K. L. & Pregitzer, K. S. Ecosystem assembly and terrestrial carbon balance under elevated CO_2. *Trends Ecol. Evol.* **22,** 538–547 (2007).

10. Nowak, R. S., Ellsworth, D. S. & Smith, S. D. Functional responses of plants to elevated atmospheric CO_2 -do photosynthetic and productivity data from

FACE experiments support early predictions? *New Phytol.* **162,** 253–280 (2004).

11. Morgan, J. A. *et al.* Water relations in grassland and desert ecosystems exposed to elevated atmospheric CO_2. *Oecologia* **140,** 11–25 (2004).

12. Raz-Yaseef, N., Rotenberg, E. & Yakir, D. Effects of spatial variations in soil evaporation caused by tree shading on water flux partitioning in a semi-arid pine forest. *Agric. For. Meteorol.* **150,** 454–462 (2010).

13. Douville, H., Ribes, A., Decharme, B., Alkama, R. & Sheffield, J. Anthropogenic influence on multidecadal changes in reconstructed global evapotranspiration. *Nat. Clim. Chang.* **3,** 59–62 (2013).

14. Ukkola, A. M. & Prentice, I. C. A worldwide analysis of trends in water-balance evapotranspiration. *Hydrol. Earth Syst. Sci.* **17,** 4177–4187 (2013).

15. Myneni, R. B. & Williams, D. L. On the Relationship between FAPAR and NDVI. *Remote Sens. Environ.* **49,** 200–211 (1994).

16. Lu, H., Raupach, M. R., McVicar, T. R. & Barrett, D. J. Decomposition of vegetation cover into woody and herbaceous components using AVHRR NDVI time series. *Remote Sens. Environ.* **86,** 1–18 (2003).

17. Hunt, E. R. Relationship between woody biomass and PAR conversion efficiency for estimating net primary production from NDVI. *Int. J. Remote Sens.* **15,** 1725–1729 (1994).

18. De Jong, R., de Bruin, S., de Wit, A., Schaepman, M. E. & Dent, D. L. Analysis of monotonic greening and browning trends from global NDVI time-series. *Remote Sens. Environ.* **115,** 692–702 (2011).

19. Beck, H. E. *et al.* Global evaluation of four AVHRR–NDVI data sets: Intercomparison and assessment against Landsat imagery. *Remote Sens. Environ.* **115,** 2547–2563 (2011).

20. Glenn, E. P., Huete, A. R., Nagler, P. L. & Nelson, S. G. Relationship between remotely-sensed vegetation indices, canopy attributes, and plant physiological

processes: what vegetation indices can and cannot tell us about the landscape. *Sensors* **8,** 2136–2160 (2008).

21. Ehleringer, J. R., Cerling, T. E. & Helliker, B. R. C_4 photosynthesis, atmospheric CO_2, and climate. *Oecologia* **112,** 285–299 (1997).

22. Le Quéré, C. *et al.* Trends in the sources and sinks of carbon dioxide. *Nat. Geosci.* **2,** 831–836 (2009).

23. Poulter, B. *et al.* Contribution of semi-arid ecosystems to interannual variability of the global carbon cycle. *Nature* **509,** 600–603 (2014).

Methods

Core datasets

Normalised Difference Vegetation Index. We obtained a time series of third-generation NDVI (NDVI3g) from the Global Inventory Modelling and Mapping Studies (GIMMS)[24]. This dataset is gridded at 0.083° spatial resolution and was averaged from biweekly to annual time steps. The annual average for a given grid cell was determined only if >80% of biweekly values were available and was set to missing otherwise. Similarly, pixel trends were only calculated for pixels with annual time series >80% complete. Basin-specific NDVI values were obtained by averaging gridded data over basin areas.

Climatic variables. Monthly climatic fields (precipitation, minimum and maximum air temperature and shortwave radiation) were obtained from the ANUCLIM archive[25]. The Australia-wide data are gridded at 0.05° spatial resolution and were produced by the ANUSPLIN software package[25,26] from meteorological station data using a thin-plate smoothing spline.

Annual time series of atmospheric CO_2 concentrations was obtained from National Oceanic & Atmospheric Administration Earth System Research Laboratory (NOAA ESRL; www.esrl.noaa.gov/gmd/ccgg/trends/). The data report the mean annual CO_2 concentration measured at Mauna Loa observatory in parts per million. We ignored latitudinal differences in CO_2 concentration as these are small compared to the signal of interest.

Potential evapotranspiration (PET) was calculated using the Priestley-Taylor method as in Gallego-Sala *et al.* (2010)[27], using inputs of shortwave radiation and the mean of minimum and maximum air temperature from the ANUCLIM archive. The Priestley-Taylor method has been shown to be appropriate for estimating large-scale PET[28,29] and has been adopted in other basin-scale studies[14,30,31].

Water-balance evapotranspiration. Water-balance evapotranspiration was calculated as the difference of observed annual precipitation and streamflow integrated over the river basin area. The water-balance method remains the most firmly observationally-based estimator of ET, but assumes negligible changes in soil water storage at annual to decadal time scales (see Supplementary Section 1 for

further discussion). Streamflow time series were acquired from the Zhang *et al.* (2013)[32] streamflow collation for unregulated catchments across Australia. Gaps in the water-balance ET time series (accounting for <5% of monthly records) were filled using simulations from the Australian Water Availability Project[33], further detailed in Supplementary Section 1.

Study basins. The 190 study basins were chosen based on the completeness of streamflow records (> 95%) and the extent of irrigated and farmed land (< 5% of basin area). The basins were classified into wet, sub-humid, semi-arid and arid using the climatological aridity index *A* (*A* = *PET*/*P*, where *PET* = annual mean potential ET and *P* = annual mean precipitation) (see Supplementary Figure 1 for basin locations and aridity classification). River basins with mean annual aridity index <1 were classified as wet, 1-2 as sub-humid, 2-5 as semi-arid and >5 as arid (adapted from UNEP (1997)[34]). See Supplementary Section 1 for further details on basin selection and classification criteria.

Breakpoint regression

Five-year running mean NDVI values were binned according to their corresponding precipitation values. Following Donohue et al. (2013)[6], the 95th percentile value was determined for each 20 mm wide precipitation bin separately for each running mean. Breakpoint regression was applied to the 95th percentile values to calculate the first regression slope marking the maximum NDVI attainable for a given precipitation and the breakpoint where the vegetation-precipitation relationship plateaus and vegetation ceases to be water-limited. We then constructed time series of the slopes and breakpoints (Figure 3) and determined linear trends for both variables. As running means were used to construct the time series, degrees of freedom were adjusted when determining the significance of trends. Farmlands, irrigated areas and wetlands were excluded from this analysis using the Dynamic Land Cover Dataset of Australia[35] (see Supplementary Section 1).

CO_2 sensitivity coefficients

Estimation of observed CO2 coefficients. Dimensionless CO_2 sensitivity coefficients were calculated from NDVI and ET corrected for precipitation and PET (a function of temperature and shortwave radiation). Precipitation and PET present the main climatic constraints on plant growth[36] and are the two first-order controls on

ET[37]. The effects of precipitation and PET were removed using linear regression: separately for each basin, annual ET (E) and NDVI were regressed against precipitation and PET and the annual corrected values were calculated as the sum of regression residual and the 1982-2010 mean of the variable. The corrected annual variables were then log-transformed and regressed against log-transformed annual CO_2 concentrations (C_a) to derive the CO_2 sensitivity coefficients $\sigma_{ET} = \partial \ln E / \partial \ln C_a$ and $\sigma_{NDVI} = \partial \ln NDVI / \partial \ln C_a$. The sensitivity coefficients represent the fractional change in the relevant variable per unit fractional change in CO_2, so that a change in ET (mm) due to CO_2 is well approximated by $\Delta E/E \approx \sigma_E . \Delta C_a/C_a$ for $\Delta E << E$ and $\Delta C_a << C_a$ (as in this study). ET and NDVI sensitivities to precipitation were calculated from uncorrected data using the same principles (further detailed in Supplementary Section 2).

Prediction of theoretical ET sensitivity to CO_2. Theoretical sensitivity of ET (E) to CO_2 concentration (C_a) for C_3 photosynthesis on a unit leaf area basis can be calculated by writing the CO_2 assimilation rate (A) and E in the form of diffusion equations:

$$A = g_s C_a (1 - \chi) \quad (1)$$

and

$$E = 1.6\, g_s D \quad (2)$$

where g_s is the stomatal conductance to CO_2, χ is the ratio of internal CO_2 concentration (C_i) to C_a, and D is the vapour pressure deficit. χ is a function of D and leaf temperature[38,39] and typically takes values from 0.4-0.5 in arid climates to 0.8-0.9 in wet climates. Substitution of g_s from equation (1) into equation (2) yields

$$E = 1.6 (D/C_a) A/(1 - \chi) \quad (3)$$

Differentiating with respect to C_a, holding D and χ constant, gives:

$$\sigma_{ET} = (C_a/E)\, \partial E/\partial C_a = \sigma_A - 1 \quad (4)$$

where σ_A is the sensitivity of A to C_a:

$$\sigma_A = (C_a/A)\, \partial A/\partial C_a \quad (5)$$

Equation (4) implies that the sensitivity of E to C_a approaches –1 as the CO_2 fertilization effect on A saturates. However, so long as A is increasing with C_a, the sensitivity is smaller in magnitude than –1. The sensitivity of A to C_a can be calculated conservatively by invoking the co-ordination hypothesis (approximate equality of the carboxylation- and electron transport-limited rates of photosynthesis under field conditions: see e.g. Maire *et al.* (2012)[40]). With the further assumption that limitation by the maximum rate of electron transport (J_{max}) is not relevant in the field (because Rubisco limitation takes over at the highest light levels), we can express the assimilation rate as

$$A = \varphi_0 I_{abs} (C_i - \Gamma^*/C_a)/(C_i + 2\Gamma^*/C_a) \quad (6)$$

where φ_0 is the intrinsic quantum efficiency of C_3 photosynthesis, I_{abs} is the absorbed photosynthetic photon flux density and Γ^* is the photorespiratory compensation point. Differentiating A with respect to C_a, holding χ constant, gives:

$$\sigma_A = \Gamma^*/C_a [1/(\chi - \Gamma^*/C_a) + 2/(\chi + 2\Gamma^*/C_a)] \quad (7)$$

Evaluating equations (7) and then (4) at 25˚C, C_a = 370 ppm for illustration gives σ_E = –0.61 for χ = 0.8 and –0.38 for χ = 0.5.

References

24. Pinzon, J. E. & Tucker, C. J. A non-stationary 1981-2012 AVHRR NDVI3g time series. *Remote Sens.* **6,** 6929–6960 (2014).

25. Xu, T. & Hutchinson, M. F. New developments and applications in the ANUCLIM spatial climatic and bioclimatic modelling package. *Environ. Model. Softw.* **40,** 267–279 (2013).

26. Kesteven, J. L. & Landsberg, J. J. *Developing a national forest productivity model. Technical report no.23, National Carbon Accounting System*. 1–102 (2004).

27. Gallego-Sala, A. *et al.* Bioclimatic envelope model of climate change impacts on blanket peatland distribution in Great Britain. *Clim. Res.* **45,** 151–162 (2010).

28. Raupach, M. R. Equilibrium evaporation and the convective boundary layer. *Boundary-Layer Meteorol.* **96,** 107–141 (2000).

29. Raupach, M. R. Combination theory and equilibrium evaporation. *Q. J. R. Meteorol. Soc.* **127,** 1149–1181 (2001).

30. Guerschman, J. P. *et al.* Scaling of potential evapotranspiration with MODIS data reproduces flux observations and catchment water balance observations across Australia. *J. Hydrol.* **369,** 107–119 (2009).

31. Zhang, L. *et al.* A rational function approach for estimating mean annual evapotranspiration. *Water Resour. Res.* **40,** W02502 (2004).

32. Zhang, Y. *et al. Collation of Australian modeller's streamflow dataset for 780 unregulated Australian catchments*. 1–115 (CSIRO Water for a Healthy Country Flagship Report, 2013).

33. Raupach, M. R. *et al. Australian Water Availability Project (AWAP): CSIRO Marine and Atmospheric Research Component: Final Report for Phase 3*. (2009).

34. UNEP (United Nations Environment Programme). *World Atlas of Desertification*. 182 (1997).

35. Lymburner, L. *et al. The National Dynamic Land Cover Dataset*. 1–95 (Geoscience Australia, 2011).

36. Nemani, R. R. *et al.* Climate-driven increases in global terrestrial net primary production from 1982 to 1999. *Science.* **300,** 1560–1563 (2003).

37. Zhang, Y. *et al.* Decadal Trends in Evaporation from Global Energy and Water Balances. *J. Hydrometeorol.* **13,** 379–391 (2012).

38. Medlyn, B. E. *et al.* Reconciling the optimal and empirical approaches to modelling stomatal conductance. *Glob. Chang. Biol.* **17,** 2134–2144 (2011).

39. Prentice, I. C., Dong, N., Gleason, S. M., Maire, V. & Wright, I. J. Balancing the costs of carbon gain and water transport: testing a new theoretical framework for plant functional ecology. *Ecol. Lett.* **17,** 82–91 (2014).

40. Maire, V. *et al.* The coordination of leaf photosynthesis links C and N fluxes in C_3 plant species. *PLoS One* **7,** e38345 (2012).

Figures

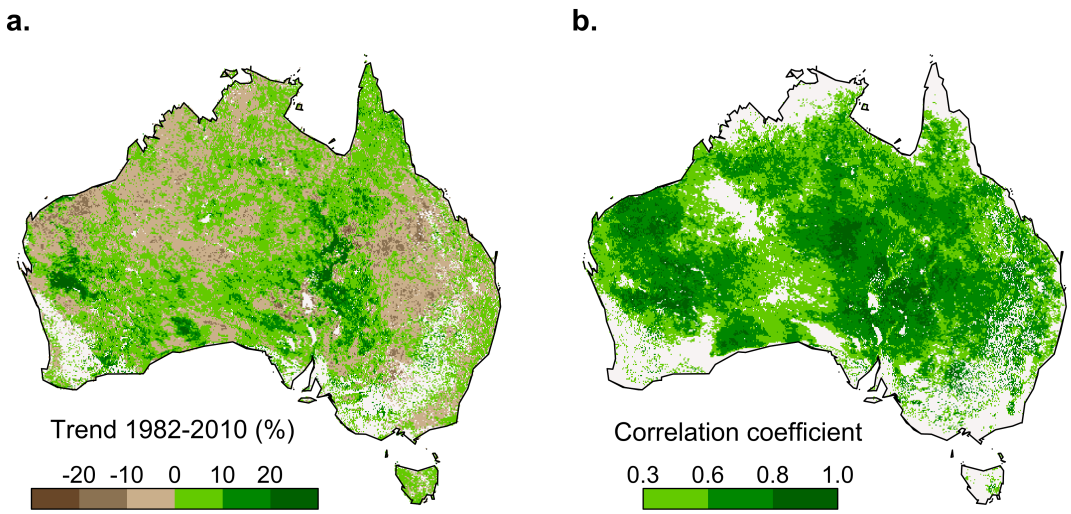

Figure 1 | Spatial patterns of vegetation greening. a, Pixel-by-pixel linear trends in annual NDVI. **b,** Areas of water-limited vegetation, determined as pixels with significant ($P \leq 0.10$) positive annual NDVI-precipitation correlations. Non-significant or negative correlations were masked out from panel b. Farmlands, irrigated areas and wetlands have been masked out from both panels.

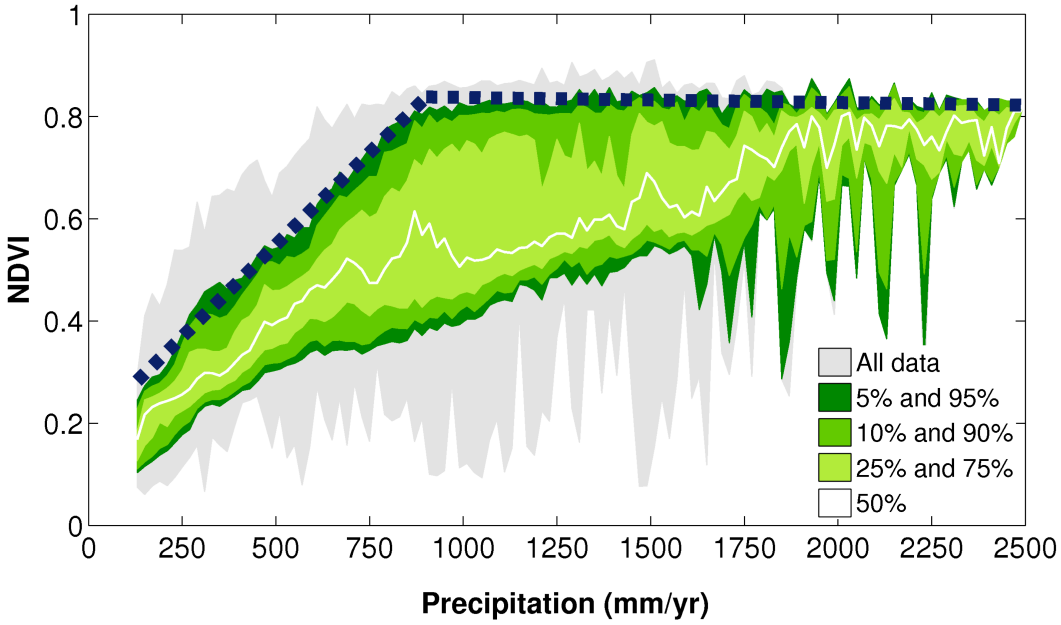

Figure 2 | Illustration of the breakpoint regression method. The first regression line represents the maximum NDVI attainable for a given amount of precipitation, under water-limited conditions. The breakpoint signifies the threshold where vegetation ceases to be water-limited. The data are the running mean 1983-1987. The coloured bands show the different percentiles.

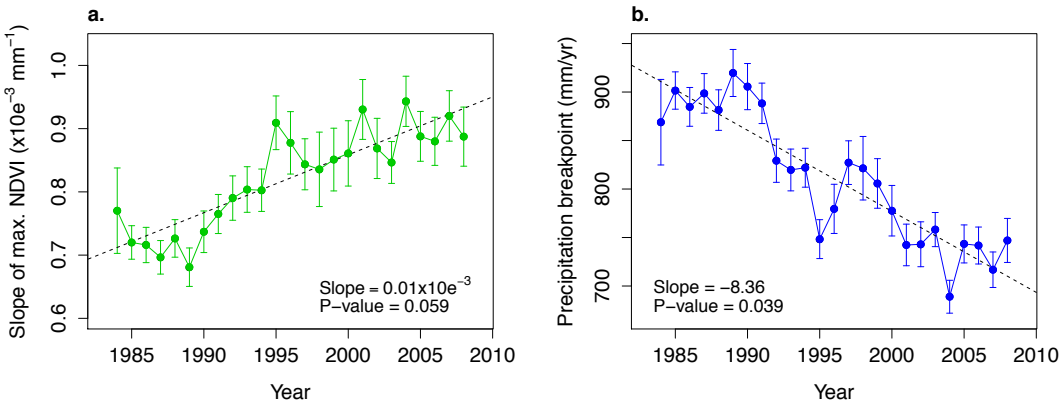

Figure 3 | Trends in water limitation threshold characteristics. a, the initial slope of maximum NDVI versus precipitation. **b,** the breakpoint (the precipitation level above which vegetation is no longer water-limited). Error bars are 95% confidence intervals. The black dashed lines show fitted linear trends.

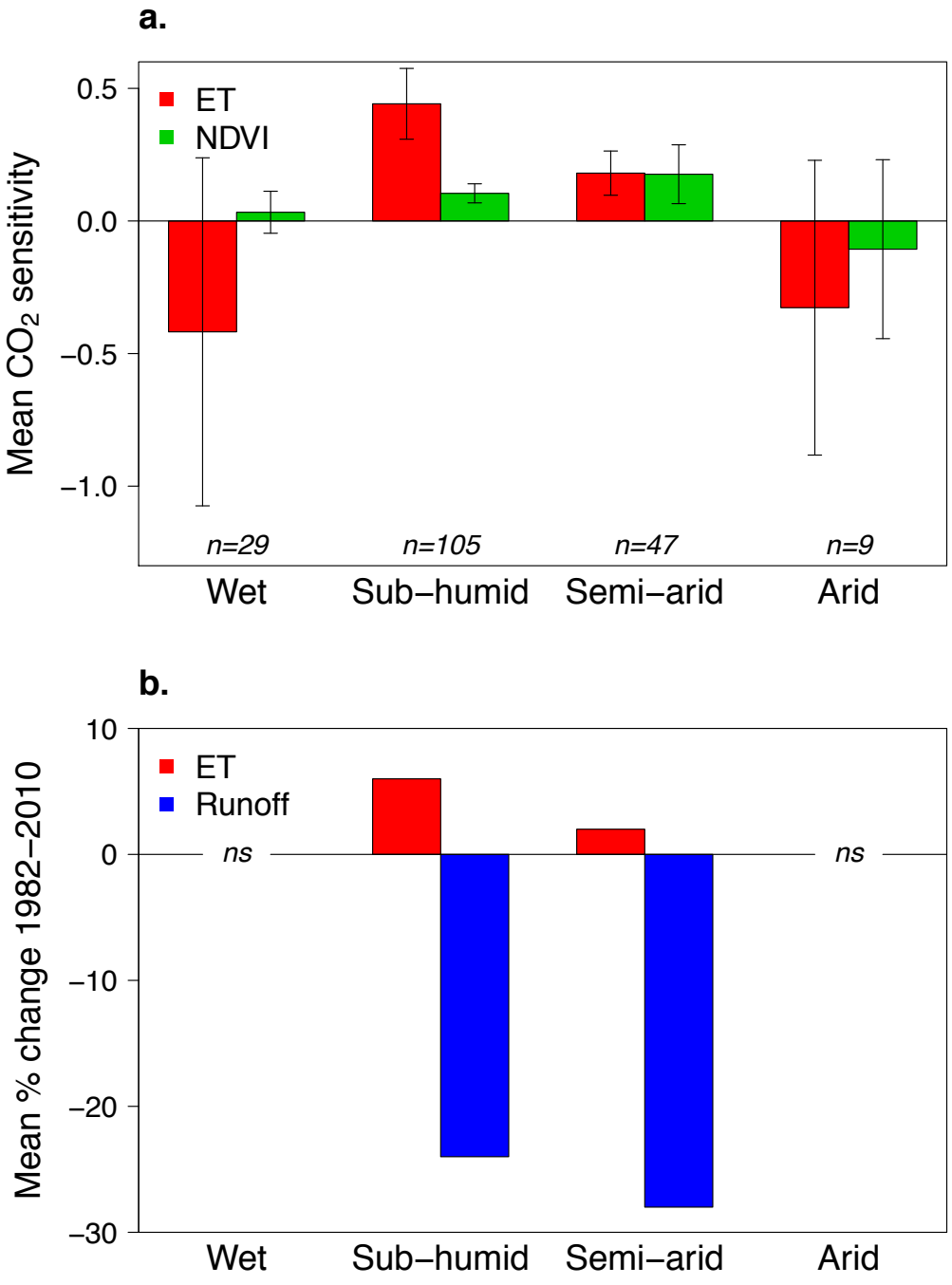

Figure 4 | CO_2 effects on ET, NDVI and runoff. a, Mean CO_2 sensitivity coefficients for each group of basins. The error bars are 95% confidence intervals. **b,** Relative change in ET and runoff due to CO_2 increase during 1982-2010. Non-significant (*ns*) changes in wet and arid basins were not shown.